



Article

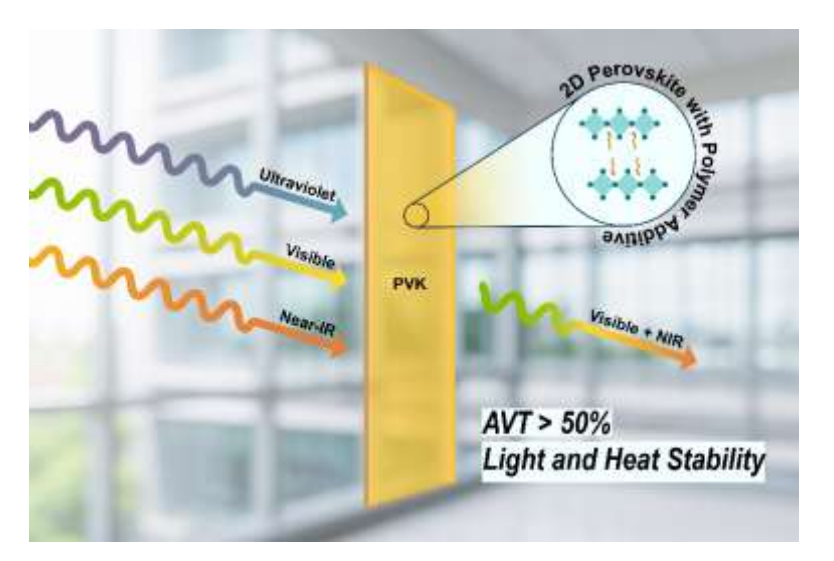
2D Ruddlesden-Popper Perovskites with Polymer Additive as Candidates for Stable and Transparent Building-Integrated Photovoltaic Materials

Adianne Alamban 1, Muneeza Ahmad 1 and Nicholas Rolston 1*

¹Renewable Energy Materials and Devices Lab, School of Electrical, Computer and Energy Engineering (ECEE), Arizona State University, Tempe, AZ, USA

Abstract: We report on the use of 2D Ruddlesden-Popper (RP) perovskites for building-integrated photovoltaics (BIPV), addressing the challenge of balancing transparency, photoluminescence, and stability. With the addition of polyvinylpyrrolidone (PVP), the 2D RP films exhibit superior transparency compared to their 3D counterparts with an average visible transmittance (AVT) greater than 50% and photoluminescence stability under continuous illumination and under 85°C heat for up to 100 hours as bare, unencapsulated films. Structural investigations show a stress relaxation in the 3D perovskite films after degradation from thermal aging that is not observed in the 2D RP films, which retain their phase after thermal and light aging. We also demonstrate ultrasmooth, wide bandgap 2D Dion-Jacobson (DJ) films with PVP incorporation up to 2.95 eV and an AVT above 70% and roughnesses of ~2 nm. These findings contribute to the development of next-generation solar materials, paving the way for their integration into built structures.

Graphical Abstract



Keywords: perovskite; 2-dimensional perovskite; structure; strain; semitransparent; wide bandgap

1. Introduction

Organic-inorganic metal halide perovskites are a rising class of semiconductor materials that have garnered the interest of the scientific community for next-generation

^{*} Correspondence: author and lead contact: Prof. Nicholas Rolston, Renewable Energy Materials and Devices Lab, School of Electrical, Computer, and Energy Engineering (ECEE), Arizona State University, Tempe, AZ, USA; e-mail: nicholas.rolston@asu.edu

photovoltaics (PV). Perovskite-based solar cell efficiencies have skyrocketed within the past decade, achieving a power conversion efficiency (PCE) of over 26% [1]. Furthermore, their extended carrier lifetimes, long diffusion lengths, and straightforward fabrication processes cement perovskites as ideal materials for PV [2,3]. In addition, the tunable components of the ABX3 structure of perovskites enable engineering of the bandgap over a wide range from ~1.2 eV to >3 eV based on the components used [4]. This tunability poses exciting potential for implementation in building-integrated photovoltaics (BIPV), a subclass of PV systems that integrate into built structures such as facades, roofs, or windows [5]. BIPV is a unique application area that distinguishes perovskites from commercialized PV technologies such as silicon and CdTe, whose optical properties are challenging to tune [6]. Other types of systems, such as organic-based PV (OPV) [7–11], have gained traction in the world of BIPV, with start-up companies pushing toward commercialization based on patents in this area [12,13]. Recent work on OPV has shown the capability for achieving respectable efficiencies and high fill factors [14]. However, these may involve vacuumbased processing routes with custom-synthesized, expensive organic precursor materials. In contrast, perovskites offer ease and rapidity of fabrication, low-cost starting materials, and highly tunable bandgap. As such, perovskites emerge as promising contenders for developing semitransparent solar windows [15].

Recent advancements in semitransparent solar cells have expanded their capabilities beyond traditional PV applications. One such avenue is the development of perovskite/organic tandem solar cells, utilizing multiple absorbers that capture both near-infrared (NIR) and ultraviolet (UV) wavelengths. This approach allows for the collection of a broader range of the electromagnetic spectrum, theoretically enhancing the overall power conversion efficiency [16]. Moreover, advancements in flexible BIPV devices [17] could enable their use on irregular and non-flat surfaces, such as car roofs, paving the way for innovative solar solutions in diverse settings. Additionally, researchers have focused on altering the color of semitransparent solar cells [18], offering the ability to tune aesthetic properties while maintaining functionality. This capability has practical applications in agrivoltaics, where semitransparent solar cells can be integrated into greenhouse systems to selectively transmit wavelengths of light conducive to plant growth while absorbing the rest, optimizing energy utilization in agricultural settings [19].

At higher bandgaps of ~2 eV, there is a significant increase in transparency while maintaining a theoretical Shockley-Queisser power conversion efficiency of >20% [20]. Achieving higher bandgap perovskite films is commonly done through partial X-site substitution of iodine with a smaller bromine anion with a smaller ionic radius [21]. However, mixed halide iodide-bromide perovskites routinely face halide segregation under light exposure and susceptibility to moisture and heat-based decomposition [22,23]. The perovskite material's propensity to degrade is a significant barrier to its widespread adoption as a PV technology. This is particularly true for BIPV applications, as building-integrated solar modules must have comparable lifetimes with window glass—about 20 years—to be commercially viable. To that end, a large and growing body of research demonstrates that two-dimensional (2D) perovskites exhibit enhanced stability compared to 3D perovskites [24]. This is in part due to mechanisms such as surface passivation, moisture resistance, and ion migration suppression characteristics brought on by the presence of bulky spacer cations in the perovskite structure [25].

In these 2D perovskites, large organic spacer cations form hydrogen bonds by intercalating between slabs of inorganic lead iodide octahedra, forming a layered perovskite structure (**Fig 1**). The "n" value represents the layers of lead iodide octahedra between cation layers. In this study, n = 1 perovskites are used for both their increased bandgap — therefore transparency—and improved stability [26]. For Ruddlesden-Popper (RP) phase perovskites, the monoammonium group in the spacer cation (n-butylammonium, BA, in this study) participates in hydrogen bonding, with Van der Waals forces interacting between cation layers [27]. For Dion-Jacobson (DJ) phase perovskites, a diammonium spacer cation (propane-1,3-diammonium, PDA, in this study) facilitates stronger hydrogen

bonding between inorganic layers (**Fig 1**). Because of the bilateral hydrogen bonds present in diammonium-containing compositions, DJ perovskites are sometimes considered to be more structurally stable than RP [27]. However, published results reveal that this is not absolute and that trade-offs in cation engineering for RP and DJ exist [24]. Nevertheless, 2D spacer cations demonstrate markedly improved operational and mechanical stability compared to 3D perovskites, particularly the n = 1 composition [26]. The key challenge for PV devices with 2D perovskites is to control the orientation of the layer such that the spacer cation does not hinder vertical charge transport, although processing strategies such as hot casting have been demonstrated to preferentially control the orientation [28].

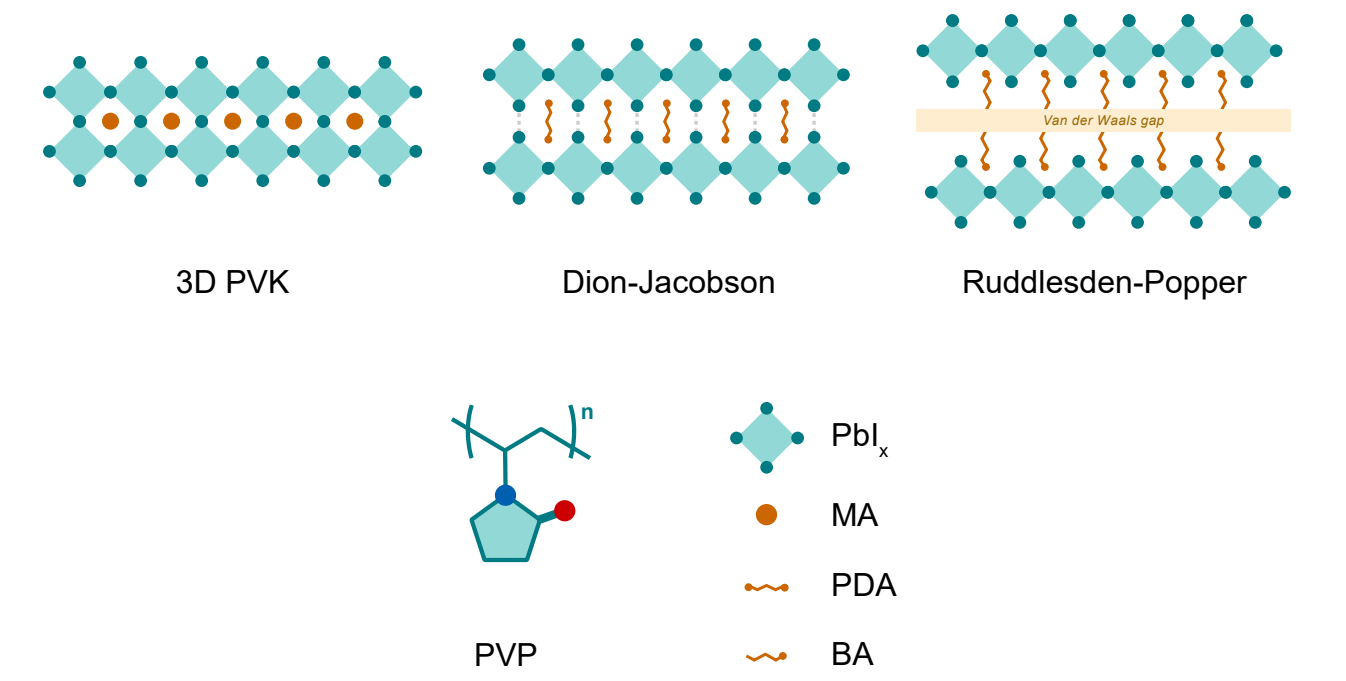


Figure 1. Schematic of the structure of 3D perovskites, n = 1 DJ and n = 1 RP perovskites, and the polymer additive PVP, respectively. The gray dashed lines in the DJ schematic represent hydrogen bonding between slabs of lead iodide octahedra. The blue and red dots in the PVP schematic denote nitrogen and oxygen heteroatoms, respectively.

Additionally, additive engineering can be leveraged to further enhance the perovskite stability. The inclusion of the polymer polyvinylpyrrolidone (PVP) has been proven to induce compressive film stresses in CsPbI₃ perovskite solar cells—a desirable effect associated with defect-healing properties [29]. Among mixed-halide perovskites such as CH₃NH₃PbI_{3-x}Cl_x, the presence of PVP is known to mitigate perovskite decomposition into PbI₂ when the film is subjected to heat and moisture [30].

To holistically evaluate the effects of compositional, dimensional, and additive engineering on the absorber material within a perovskite solar cell, we posit the use of three interrelated metrics: Transparency, Efficiency, and STability (TEST) (Fig 2). By examining these characteristics, we aim to understand which absorber composition and structure will be most well-suited for BIPV windows. The materials used in these devices must be transparent enough to let in ambient light to illuminate the inside of the building, which is quantified using UV-Vis spectroscopy. Additionally, to function as a light absorber, the material must also be able to generate electron-hole pairs from exposure to light. This is quantified using steady-state photoluminescence (PL). Lastly, to compete with conventional windows, a stable material that can withstand environmental stressors is imperative. Accelerated light and heat aging studies are performed to illustrate this with unencapsulated films. Ultimately, an effective absorber material for BIPV windows must perform well in all 3 of the TEST criteria to be considered as a potential candidate. Of

117

118

119

120

121

122

123

124

125

126

127

128

129

130

131

132

133

134

135

136

137

138

course, there remain additional challenges in interface and device engineering that need to then be considered as well, but for this study, film-level understanding remained the focus.

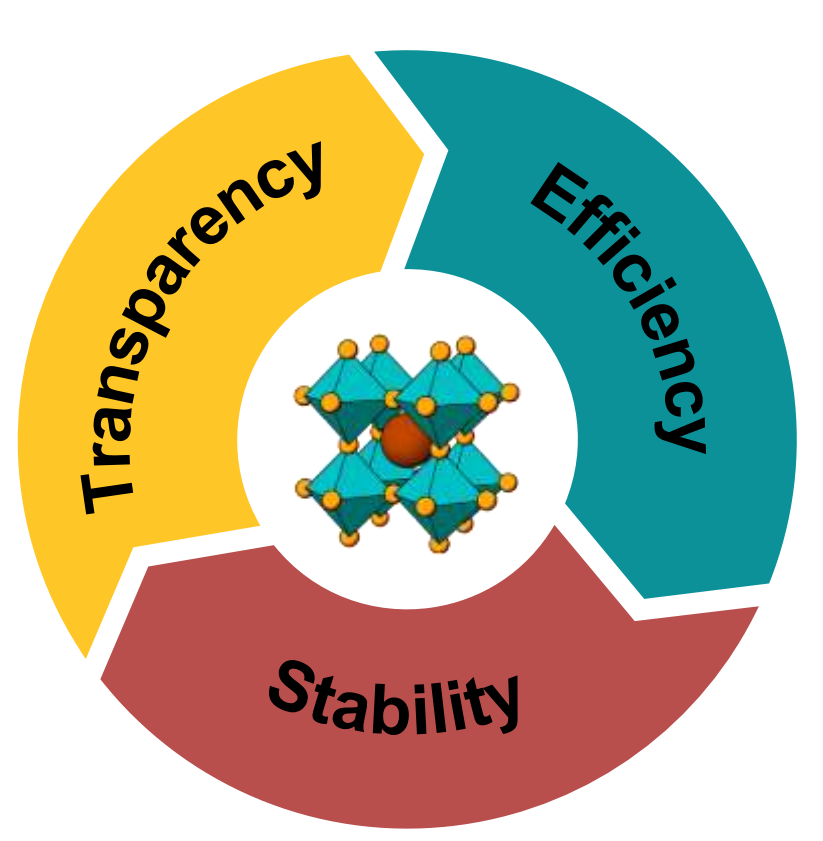


Figure 2. Transparency, Efficiency, and STability (TEST) Criteria. Suitability of BIPV absorber materials were gauged via these three characteristics.

2. Results

A one-step spin coating process without quenching was used to produce uniform films of both n=1 DJ (PDAPbI4) and n=1 RP ((BA)2PbI4) perovskites featuring good surface coverage and no discernable pinholes. Despite employing the commonly used antisolvent method [31] for the 3D mixed-halide samples (MAPbBr1.5I1.5), localized islands of nonuniformity remained (Fig. 3a). These features are likely caused by nonuniform crystallization and were not present in either the DJ or RP films, a challenge which has been well-documented for mixed-halide 3D perovskite films [32]. For the RP film in Fig. 3b, features tens of microns across can be observed, which are not visually evident in the RP-PVP films (Fig. 3c). Guo et al. suggest that this may be due to the PVP causing the perovskite to form nanocrystals which result in smaller surface features [30]. These features are small enough such that they are indistinguishable at millimeter length scales. Consequently, this resulted in a reduction in the roughness of the RP-PVP and DJ-PVP films, with the DJ-PVP films reaching an extremely low roughness of 2 nm (Fig. S1). In addition to reducing the roughness, PVP increased the perovskite film thickness (Fig. S2). For both DJ-PVP and RP-PVP samples, adding PVP resulted in films roughly 100 nm thicker than without it. Thickness and roughness values are summarized in Fig. 3f.

140

141

142

143

144

145

146

148

149

150

151

152

153

154

155

156

157

158

159

160

161

162

163

164

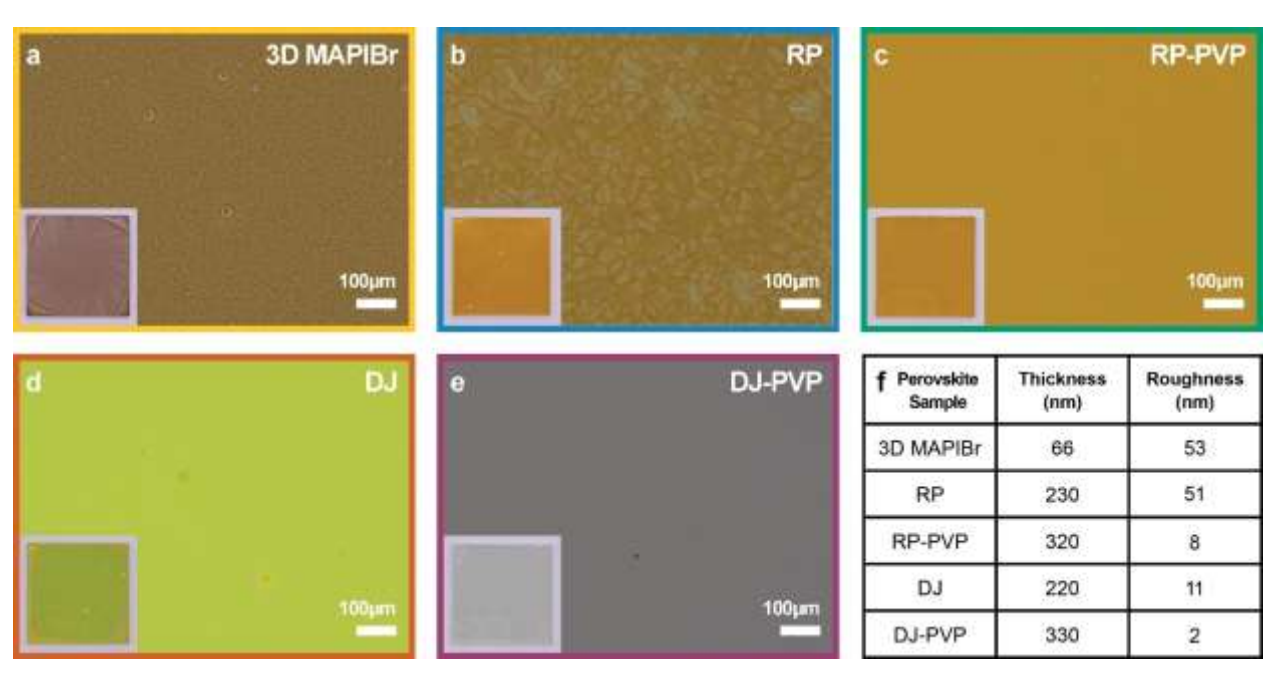


Figure 3. Morphology, Thickness, and Roughness. **a-e** Optical microscope images of 3D, RP, RP-PVP, DJ, and DJ-PVP films, respectively. Inset are camera images of the 1"x1" samples. **f** Table of thickness and roughness values for each sample.

While the 3D films were the characteristic brown color of mixed-halide perovskites [21], the RP films exhibited a mild orange color—regardless of whether PVP was added. However, for the DJ films, a drastic color change from neon green (**Fig. 3d**) to nearly transparent (**Fig. 3e**) can be seen when incorporating the additive, an effect which is attributed to the increased bandgap of the DJ-PVP films [4]. This shows the potential for using 2D perovskites in designing BIPV for aesthetics with compositional tuning to adjust the color.

The color and transparency changes observed in the films were measured with UV-Vis spectroscopy (Fig. 4a). In the absorption and transmission spectra of the DJ and RP films, oscillations can be observed, which may be attributed to interference effects (Fig. S3). Additionally, they displayed a much higher transmittance than their 3D counterpart, which had the poorest average visible transmittance (AVT) of 31%. In contrast, the DJ film had a reasonable AVT of 55%, which increased to 72% AVT with the DJ-PVP. The increased transparency was met with an expected blue-shift in the bandgap from 2.63 eV to 2.95 eV, as derived from Tauc plots of the absorbance data. The RP films reached an AVT of 47%, which increased to 54% AVT with the RP-PVP films. These RP and RP-PVP samples exhibited similar absorption profiles for the sub-523 nm wavelengths (Fig. 4a). For longer wavelengths, however, RP-PVP samples had improved transmission, resulting in nearly a 10% increase in AVT compared to the RP. Despite the difference in AVT, there was no significant change in the bandgap energy between the two types of RP films, with RP and RP-PVP films having a measured bandgap of 2.37 eV and 2.38 eV, respectively. As such, it appears that the PVP has a more prominent role in affecting the DJ structure than the RP perovskite.

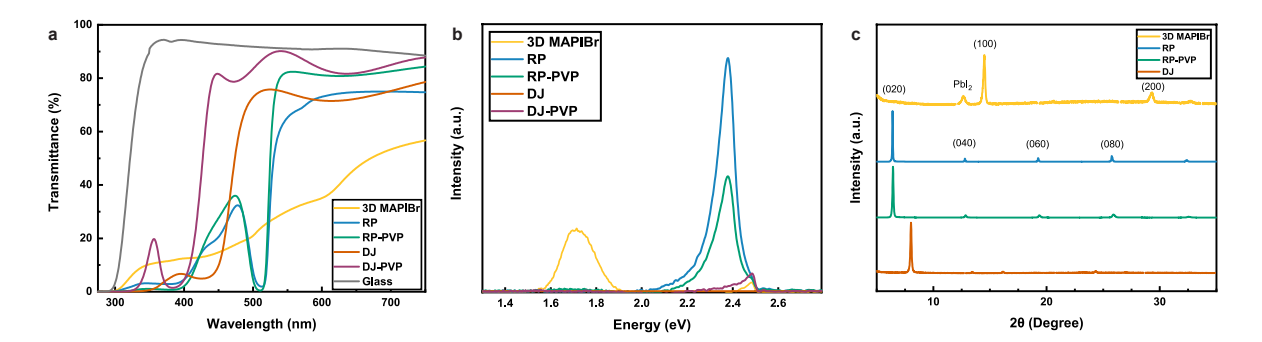


Figure 4. Optoelectronic and Structural Properties. **a** UV-Vis transmittance spectra of all five samples, including glass, were collected with air as the baseline. **b** Steady-state PL curves. **c** XRD spectra of 3D, RP, RP-PVP, and DJ samples. The DJ-PVP spectrum was not included due to issues in crystallization.

Table 1. Change in pre- and post-aging PL intensity for films aged under light and heat over a 96-hour period.

	3D MAPIBr	RP	RP-PVP
Light-aged	14% increase	25% increase	66% increase
Heat-aged	64% decrease	5% increase	29% increase

The relatively lower measured PL intensity of the 3D perovskite seen in **Fig. 4b** is likely due to a combination of reduced thickness, poorer morphology, incomplete film coverage of the substrate, and the well-documented temporal instability of the PL intensity in mixed-halide perovskites [33]. This peak instability was not observed for the pure-iodide RP samples, which is an indication of the improved optoelectronic stability of the RP perovskite. Among the RP samples, the RP-PVP exhibited a lower PL response than the RP film. Because PL intensity can be used as a proxy for electrical performance [33], we conclude that PVP slightly reduces optoelectronic response due to the insulating nature of the material. However, previous work on all-inorganic perovskite suggests that PVP-enhanced perovskite films can reap the benefits of the additive without compromising device performance [34], and tuning the concentration of the PVP is a direction that will be studied in future work.

In stark contrast, neither of the DJ samples yielded any noticeable PL response when excited with the same laser diode. Despite the remarkable transparency displayed by the DJ-PVP films, the low PL signal suggests poor light-harvesting performance in a solar device. Since a 450 nm (~2.76 eV) laser was used for excitation, it is possible that a shorter excitation wavelength would be needed to achieve a better response, particularly for the DJ-PVP sample. Nonetheless, it is important to note that at these extremely wide bandgaps, the theoretical power conversion efficiency limit is quite low (~5%).

X-ray diffraction (XRD) spectra for the RP perovskites in **Fig. 4c** show a dominant reflection of the (020) plane, with additional peaks at (040), (060), and (080), which aligns with previously reported data from Lin et al. [34]. On the subject of phase stability with the RP-PVP films, no new peaks appear—only a slight broadening likely caused by the polymer's amorphous structure. Overall, the RP phase remains intact despite the presence of PVP, an effect which shows the PVP does not disrupt the overall 2D perovskite crystallinity. This is reinforced by the unchanging bandgap that was measured with and without PVP for the RP films.

Similar to the RP films, there is also a prominent diffraction peak at low angles within the 5°-10° range for the DJ, aligning well with the structure of 2D perovskites. However, the XRD data reveals that the addition of the PVP additive to the DJ-PVP ink resulted in

films that did not crystallize to the perovskite phase. This may be studied further via concentration studies to identify an ideal concentration of PVP that maintains the desired phase; however, this was not a focus of this study since the unmodified DJ film did not show a noticeable PL response.

For the 3D spectra, there is a small PbI_2 peak observed at 12.7° , characteristic of perovskite degradation as well as poorer crystallization in the thin film (**Fig. 4c**). This is further supported by the increased peak widths in the 3D sample when compared to the spectra from the DJ and RP films.

To better understand the environmental stability characteristics of the perovskite films, they were subjected to accelerated light and heat aging. PL spectra were measured periodically in 24-hour intervals over 96 hours. Because of the minimal performance of the DJ films under PL, they were not used in this aging study. As such, the following discussion on film stability will focus on the comparison between the performance of the RP and 3D films.

The RP perovskite demonstrated superior stability over the 3D film under illumination for both RP and RP-PVP samples (**Fig. 5a-c**). The maximum intensity of the 3D PL peak begins to decrease after only 48 hours, whereas the RP continues to steadily increase over the 96-hour aging period. Additionally, the PVP serves to bolster this stability, causing a 66.8% increase in PL intensity after aging (**Fig. 5c**). The larger increase in PL may be attributable to a reduction or annihilation of trap states [35,36].

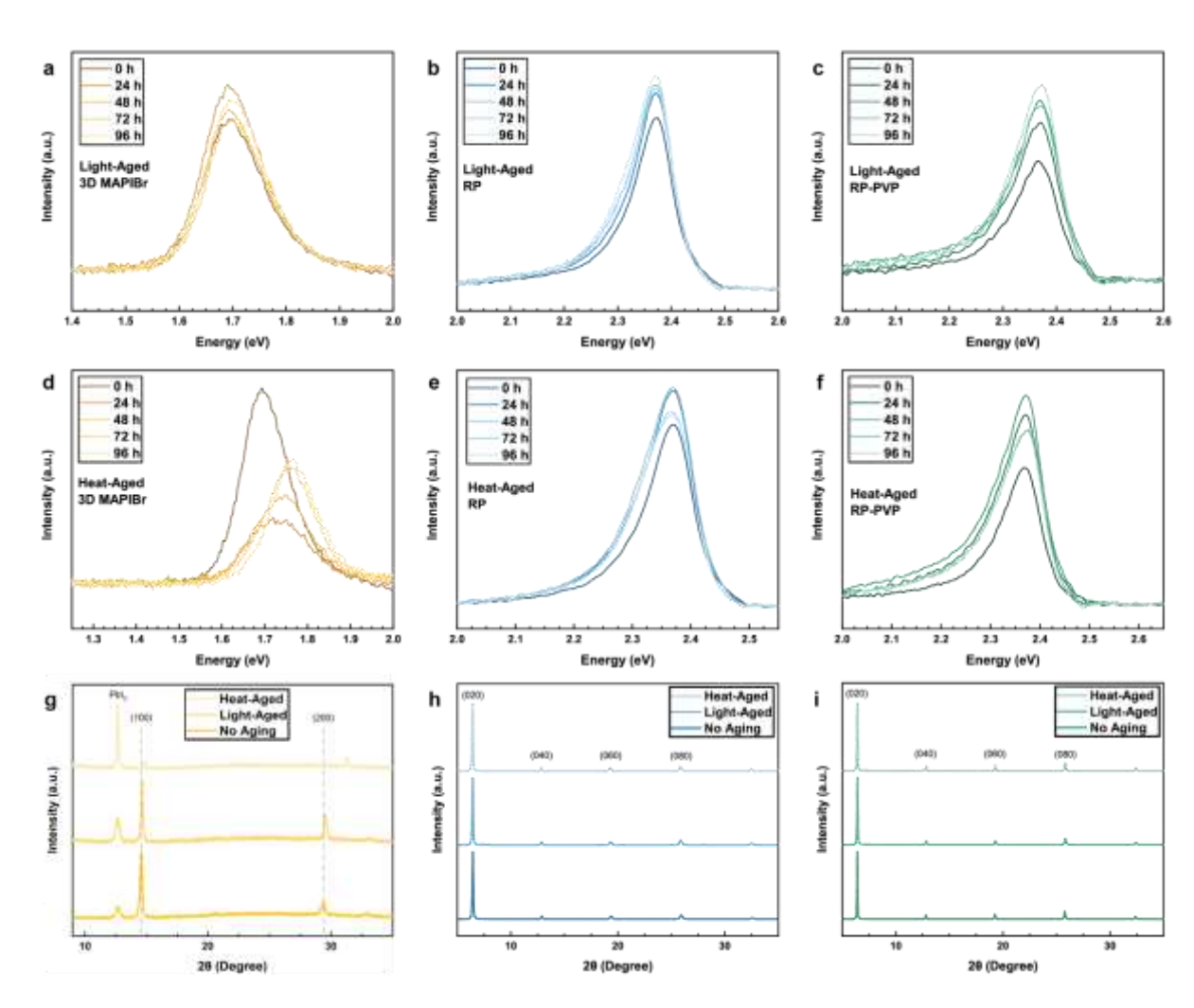


Figure 5. Light and Heat Aging Studies. **a-c** Steady-state PL spectra of 3D, RP, and RP-PVP films subject to 1 sun illumination for 96 hours, collected in 24-hour intervals. **d-e** Steady-state PL spectra

of films subject to 85°C accelerated thermal aging for 96 hours, collected in 24-hour intervals. **g-i** XRD spectra of films before and after the aging studies.

Under thermal aging, it is evident that all samples suffered from thermal exposure to high heat (**Fig. 5d-f**). The PL intensity of the 3D film diminished by 63.7% (**Fig. 5d**). This is expected, as it is well-documented that 3D perovskites are susceptible to degradation under heat [37], particularly methylammonium-based compositions used here. Further, evidence of phase segregation is observed in the blue-shift of the PL peak from 1.72 eV to 1.74 eV. As the Pb-I bonds break with increased thermal stress, the Pb-Br bonds remain, resulting in PL characteristics more aligned with that of a pure methylammonium lead bromide perovskite, thus the shift to higher energies [36].

A drastic blue-shift was not seen for either RP or RP-PVP heat-aged films, where the PL emission remained consistent at roughly 2.37 eV. Unlike the light-aged films, whose PL intensities increased steadily, the PL intensity of the heat-aged RP films began to drop after 72 hours. This indicates that the RP perovskite used in this study is more resilient to light than thermal stressors. While PVP does not solve this instability, it does, however, result in a 29% increase in intensity overall (**Fig. 5e**). In comparison, the PL increased only 5% in the absence of PVP (**Fig. 5f**). The increase in PL intensity suggests enhanced thermal stability due to the addition of PVP.

XRD spectra were collected after the aging study to complement the PL data and to analyze structural changes that may have occurred (**Fig. 5g-i**). The 3D samples experienced the most degradation due to heat. These films clearly exhibit degradation of the perovskite into lead iodide, as supported by the growth of the peak at 12.7°, particularly for the heat-aged sample. Further evidence of degradation is seen in the loss and shift of the perovskite peak originally at 14.6° in the heat- and light-aged samples, respectively (**Fig. S4**). There is also possible evidence for a stress relaxation-based degradation mode in the heat-aged sample, in particular, based on the larger shift in 20 for the (200) compared to the (100) peak.

There is no noticeable growth of the lead iodide peak at 12.7° with the RP samples, nor is there an indication of stress relaxation under either light or heat. This suggests that the RP perovskite retains its structure even after being subjected to accelerated aging. Similar results were observed in the RP-PVP, whose spectra indicate strong phase stability after aging. While there is a slight peak shift to lower 2θ , the change is negligible and on the order of hundredths of a degree (Fig. S5-6). For the RP-PVP films, in particular, the light-aged samples underwent a larger shift than those aged with heat (Table S1).

Overall, it is evident from the PL and XRD spectra that the RP thin films exhibit superior light and thermal stability when compared to traditional 3D perovskites. Their phase stability and resistance to degradation are ideal for their use in BIPV.

To summarize our findings, we developed a metric that visually represents the suitability of the materials we studied for BIPV windows based on the TEST Criteria (**Fig. 6**). The RP films yielded the best balance among the three—achieving respectable transparency, great PL, and strong phase stability under light and heat. On the other hand, the DJ and 3D films were deemed less suitable for their poor PL and stability characteristics, respectively.

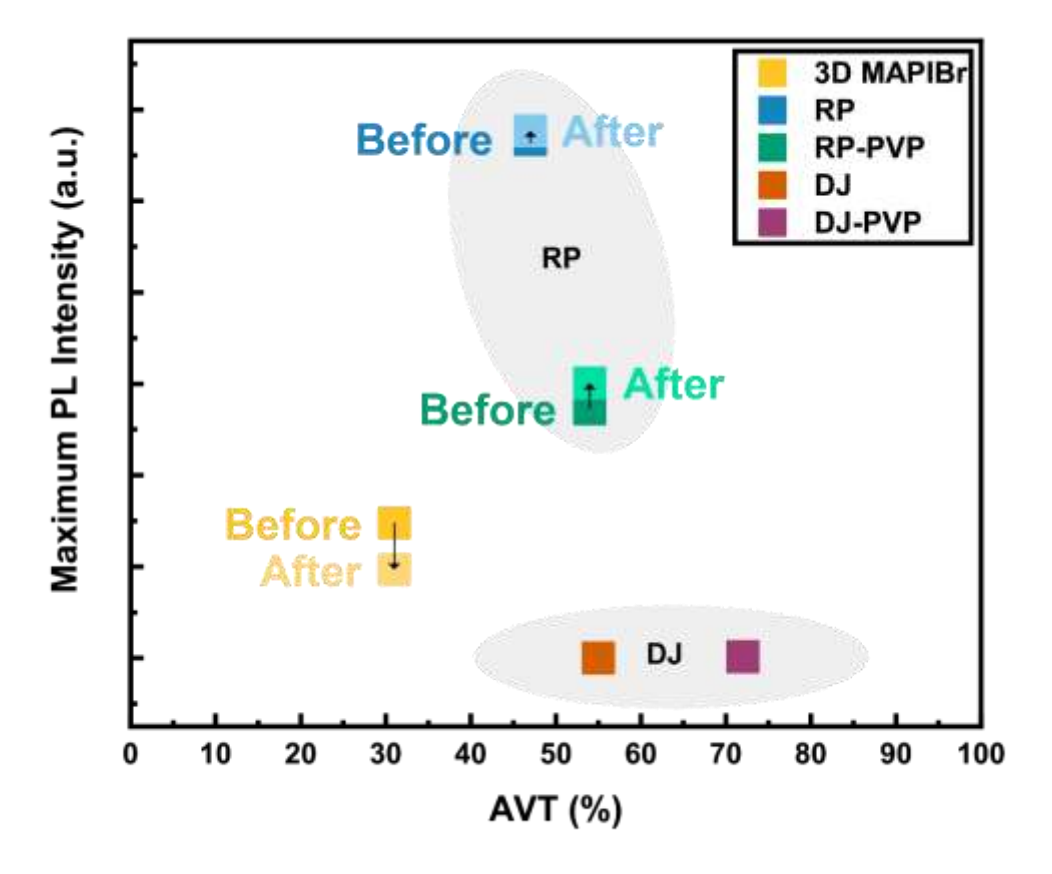


Figure 6. The Metric. A visual representation of the candidate materials' suitability for BIPV windows based on the TEST Criteria. Maximum PL intensities vs. AVT for each sample are plotted both before and after aging with heat (85°C) and demarcated accordingly.

3. Discussion

In this work, we leveraged the TEST Criteria to evaluate the suitability of DJ and RP perovskite materials for their use in BIPV. Ultimately, we propose the use of RP phase 2D perovskites with a PVP additive as a promising candidate for the absorber material in BIPV applications. While the DJ films held a higher AVT, the trade-off lies in their weak PL characteristics. In contrast, RP-PVP films exhibited a respectable AVT (>50%) with strong PL and structural stability, as quantified by PL and XRD measurements under accelerated aging studies. In conclusion, our study highlights the potential of RP perovskites as a stable, semitransparent absorber material for BIPV. We have successfully demonstrated the viability of these perovskite compositions, although further work is needed to integrate these films into semitransparent devices effectively.

Moving forward, future experiments will focus on studying charge transport layers, electrodes, and their interfacial interactions within semitransparent perovskite PV devices. Additionally, understanding the interaction of PVP with perovskite films through concentration studies is crucial for optimizing device performance.

This study ultimately adds to the growing body of work revolving around the use of 2D/low-dimensional perovskites in PV. This not only expands the scope of semitransparent solar cells but also opens avenues for applications in agrivoltaics and energy for transportation. More stable and efficient semitransparent solar cells can unlock the potential of existing building facades and open new frontiers in the field of solar energy. Overall, our work lays the groundwork for future innovations in the field, driving us closer to ubiquitous and lasting energy solutions.

4. Materials and Methods

The RP inks were fabricated as follows. 201 mg of n-butylammonium iodide (BAI) (Greatcell Solar, >99%) and 231 mg of lead iodide (PbI2) (TCI, >98.0%) were dissolved in 400 μL of N,N-Dimethylformamide (DMF) (Sigma-Aldrich, 99.8%) and 600 μL of dimethyl sulfoxide (DMSO) (Sigma-Aldrich, ≥99.9%) to create a 0.5M solution of (BA)₂PbI₄ in 2:3 v/v DMF/DMSO. The 0.5M DJ samples were prepared in a similar fashion, dissolving 165 mg of propane-1,3-diammonium iodide (PDAI₂) (Greatcell Solar, >99.8%) and 231 mg of PbI2 in 800 µL of DMF and 200 µL of n-methylpyrrolidone (NMP) (Sigma-Aldrich, 99.5%) to create PDAPbI4 in 4:1 v/v DMF/NMP. For the samples with polyvinylpyrrolidone (PVP), 4 wt% of PVP (Sigma-Aldrich, 10 000 g/mol) was added with respect to the ink-61 mg for the RP-PVP ink and 57 mg for the DJ-PVP ink. 3D perovskites were fabricated as a basis to which the 2D samples were compared. For the 3D samples, a mixed-halide comp osition of 0.5M MAPbBr_{1.5}I_{1.5} dissolved in 4:1 v/v DMF/DMSO was used. In this solution, 40 mg of methylammonium iodide (MAI) (Greatcell Solar, >99.99%), 28 mg of methylammonium bromide (MABr) (Greatcell Solar, >99.99%), 115 mg of PbI₂, and 92 mg of lead bromide (PbBr2) (TCI, >98.0%) were dissolved in 800 µL of DMF and $200 \mu L$ of DMSO.

All films in this study were solution-processed and deposited onto 1"x1" glass substrates via spin coating in a N₂ glovebox. Prior to spinning, all substrates were preheated at 100°C for 10 mins. The films were spin-coated at 4000 rpm for 30 s, with chlorobenzene (CB) (Sigma-Aldrich, 99.8%) antisolvent dropped at 15 s for the 3D films only. After spinning, all films were annealed at 100°C for 10 mins on a hot plate. The produced films were then subject to accelerated light and heat aging under AM 1.5G illumination and 85°C, respectively, for 96 hours.

Microscope images were taken on a Keyence VHX-7000. A Cary 5000 UV-Vis-NIR spectrophotometer was used to collect absorption and transmission spectra. For the steady-state PL data, the CPS450 collimated 450 nm, 4.5 mW laser diode module was used. The Rigaku Smart Lab X-ray Diffractometer was used to gather XRD spectra.

Acknowledgments: This material is based upon work supported by the U.S. Department of Energy's Office of Energy Efficiency and Renewable Energy (EERE) under Solar Energy Technologies Office (SETO) Agreement Number DE-EE0010502. The authors also acknowledge the use of facilities within the Eyring Materials Center at Arizona State University supported in part by NNCI-ECCS-1542160. The authors acknowledge resources and support from the Advanced Electronics and Photonics Core Facility at Arizona State University. The authors thank Mason Mahaffey from Arizona State University for helpful discussions and insights.

Conflicts of Interest: The authors have no conflicts of interest to report.

Data Availability Statement: Data will be made available upon reasonable request.

Author Contributions: A.A. – Conceptualization, data curation, formal analysis, investigation, methodology, validation, visualization, writing – original draft, writing – review & editing. M.A. – Data curation, investigation, methodology, validation, writing – review & editing. N.R. – Conceptualization, funding acquisition, project administration, resources, supervision, writing – review & editing.

References

- 1. Park, J.; Kim, J.; Yun, H.-S.; Paik, M.J.; Noh, E.; Mun, H.J.; Kim, M.G.; Shin, T.J.; Seok, S. Il Controlled Growth of Perovskite Layers with Volatile Alkylammonium Chlorides. *Nature* **2023**, *616*, 724–730, doi:10.1038/s41586-023-05825-y.
- 2. Chen, Y.; Yi, H.T.; Wu, X.; Haroldson, R.; Gartstein, Y.N.; Rodionov, Y.I.; Tikhonov, K.S.; Zakhidov, A.; Zhu, X.Y.; Podzorov, V. Extended Carrier Lifetimes and Diffusion in Hybrid Perovskites Revealed by Hall Effect and Photoconductivity Measurements. *Nat Commun* **2016**, *7*, doi:10.1038/ncomms12253.

- 3. Huang, J.; He, S.; Zhang, W.; Saparbaev, A.; Wang, Y.; Gao, Y.; Shang, L.; Dong, G.; Nurumbetova, L.; Yue, G.; et al. Efficient and Stable All-Inorganic CsPbIBr2 Perovskite Solar Cells Enabled by Dynamic Vacuum-Assisted Low-Temperature Engineering. *Solar RRL* **2022**, *6*, doi:10.1002/solr.202100839.
- 4. Hu, Z.; Lin, Z.; Su, J.; Zhang, J.; Chang, J.; Hao, Y. A Review on Energy Band-Gap Engineering for Perovskite Photovoltaics. *Solar RRL* 2019, 3.
- 5. Koh, T.M.; Wang, H.; Ng, Y.F.; Bruno, A.; Mhaisalkar, S.; Mathews, N. Halide Perovskite Solar Cells for Building Integrated Photovoltaics: Transforming Building Façades into Power Generators. *Advanced Materials* **2022**, 34, doi:10.1002/adma.202104661.
- 6. Zheng, X.; Kuciauskas, D.; Moseley, J.; Colegrove, E.; Albin, D.S.; Moutinho, H.; Duenow, J.N.; Ablekim, T.; Harvey, S.P.; Ferguson, A.; et al. Recombination and Bandgap Engineering in CdSeTe/CdTe Solar Cells. *APL Mater* 2019, 7, doi:10.1063/1.5098459.
- 7. Meng, D.; Zheng, R.; Zhao, Y.; Zhang, E.; Dou, L.; Yang, Y. Near-Infrared Materials: The Turning Point of Organic Photovoltaics. *Advanced Materials* 2022, 34.
- 8. Li, G.; Zhu, R.; Yang, Y. Polymer Solar Cells. Nat Photonics 2012, 6, 153–161.
- 9. Hou, J.; Inganas, O.; Friend, R.H.; Gao, F. Organic Solar Cells Based on Non-Fullerene Acceptors. *Nat Mater* 2018, 17, 119–128.
- 10. Li, Y.; Huang, X.; Sheriff, H.K.M.; Forrest, S.R. Semitransparent Organic Photovoltaics for Building-Integrated Photovoltaic Applications. *Nat Rev Mater* **2023**, *8*, 186–201, doi:10.1038/s41578-022-00514-0.
- 11. Cui, Y.; Yao, H.; Zhang, J.; Xian, K.; Zhang, T.; Hong, L.; Wang, Y.; Xu, Y.; Ma, K.; An, C.; et al. Single-Junction Organic Photovoltaic Cells with Approaching 18% Efficiency. *Advanced Materials* **2020**, 32, doi:10.1002/adma.201908205.
- 12. DIRK, H.; OLGA, G.; ROLAND, F.; DANIEL, D.; GUNTER, M.; ANDRE, W. Organic Semiconducting Material and Use Thereof in Organic Devices 2021.
- 13. ANTOINE, M.; DANIEL, D.; ROLAND, F.; OLGA, G.; DIRK, H.; GUNTER, M.; ANDRE, W. Organic Semiconducting Material and Its Synthesis and Organic Semiconducting Component with the Material 2022.
- 14. Gao, Y.; Xiao, Z.; Cui, M.; Saidaminov, M.I.; Tan, F.; Shang, L.; Li, W.; Qin, C.; Ding, L. Asymmetric Π-Bridge Engineering Enables High-Permittivity Benzo[1,2-B:4,5-B']Difuran-Conjugated Polymer for Efficient Organic Solar Cells. *Advanced Materials* **2024**, *36*, 2306373, doi:https://doi.org/10.1002/adma.202306373.
- 15. Di Girolamo, D.; Vidon, G.; Barichello, J.; Di Giacomo, F.; Jafarzadeh, F.; Paci, B.; Generosi, A.; Kim, M.; Castriotta, L.A.; Frégnaux, M.; et al. Breaking 1.7 V Open Circuit Voltage in Large Area Transparent Perovskite Solar Cells Using Interfaces Passivation. *Adv Energy Mater* **2024**, doi:10.1002/aenm.202400663.
- 16. Rossi, D.; Forberich, K.; Matteocci, F.; Auf der Maur, M.; Egelhaaf, H.J.; Brabec, C.J.; Di Carlo, A. Design of Highly

 374

 Efficient Semitransparent Perovskite/Organic Tandem Solar Cells. Solar RRL 2022, 6, doi:10.1002/solr.202200242.

 375
- 17. Li, S.; Wang, C.; Zhao, D.; An, Y.; Zhao, Y.; Zhao, X.; Li, X. Flexible Semitransparent Perovskite Solar Cells with 376 Gradient Energy Levels Enable Efficient Tandems with Cu(In,Ga)Se2. *Nano Energy* **2020**, 78, 377 doi:10.1016/j.nanoen.2020.105378.
- 18. Wang, H.; Dewi, H.A.; Koh, T.M.; Bruno, A.; Mhaisalkar, S.; Mathews, N. Bifacial, Color-Tunable Semitransparent Perovskite Solar Cells for Building-Integrated Photovoltaics. *ACS Appl Mater Interfaces* **2020**, 12, 484–493, doi:10.1021/acsami.9b15488.
- 19. Gorjian, S.; Bousi, E.; Özdemir, Ö.E.; Trommsdorff, M.; Kumar, N.M.; Anand, A.; Kant, K.; Chopra, S.S. Progress and Challenges of Crop Production and Electricity Generation in Agrivoltaic Systems Using Semi-Transparent Photovoltaic Technology. *Renewable and Sustainable Energy Reviews* 2022, 158.

- 20. Shockley, W.; Queisser, H.J. Detailed Balance Limit of Efficiency of P-n Junction Solar Cells. *J Appl Phys* **1961**, 32, 510–519, doi:10.1063/1.1736034.
- 21. Kulkarni, S.A.; Baikie, T.; Boix, P.P.; Yantara, N.; Mathews, N.; Mhaisalkar, S. Band-Gap Tuning of Lead Halide Perovskites Using a Sequential Deposition Process. *J Mater Chem A Mater* **2014**, 2, 9221–9225, doi:10.1039/c4ta00435c.
- 22. Dong, Q.; Zhu, C.; Chen, M.; Jiang, C.; Guo, J.; Feng, Y.; Dai, Z.; Yadavalli, S.K.; Hu, M.; Cao, X.; et al. Interpenetrating Interfaces for Efficient Perovskite Solar Cells with High Operational Stability and Mechanical Robustness. *Nat Commun* **2021**, *12*, doi:10.1038/s41467-021-21292-3.
- 23. Baumann, F.; Raga, S.R.; Lira-Cantú, M. Monitoring the Stability and Degradation Mechanisms of Perovskite Solar Cells by in Situ and Operando Characterization . *APL Energy* **2023**, *1*, doi:10.1063/5.0145199.
- 24. Liu, Y.; Zhou, H.; Ni, Y.; Guo, J.; Lu, R.; Li, C.; Guo, X. Revealing Stability Origin of Dion-Jacobson 2D Perovskites with Different-Rigidity Organic Cations. *Joule* **2023**, *7*, 1016–1032, doi:10.1016/j.joule.2023.03.010.
- 25. Wu, G.; Liang, R.; Ge, M.; Sun, G.; Zhang, Y.; Xing, G. Surface Passivation Using 2D Perovskites toward Efficient and Stable Perovskite Solar Cells. *Advanced Materials* 2022, 34.
- 26. Li, M.; Johnson, S.; Gil-Escrig, L.; Sohmer, M.; Figueroa Morales, C.A.; Kim, H.; Sidhik, S.; Mohite, A.; Gong, X.; Etgar, L.; et al. Strategies to Improve the Mechanical Robustness of Metal Halide Perovskite Solar Cells. *Energy Advances* **2023**, *3*, 273–280, doi:10.1039/d3ya00377a.
- 27. Ahmad, S.; Fu, P.; Yu, S.; Yang, Q.; Liu, X.; Wang, X.; Wang, X.; Guo, X.; Li, C. Dion-Jacobson Phase 2D Layered Perovskites for Solar Cells with Ultrahigh Stability. *Joule* **2019**, *3*, 794–806, doi:10.1016/j.joule.2018.11.026.
- 28. Liao, K.; Li, C.; Xie, L.; Yuan, Y.; Wang, S.; Cao, Z.; Ding, L.; Hao, F. Hot-Casting Large-Grain Perovskite Film for Efficient Solar Cells: Film Formation and Device Performance. *Nanomicro Lett* 2020, 12.
- 29. Nguyen, H.; Penukula, S.; Mahaffey, M.; Rolston, N. All Inorganic CsPbI3 Perovskite Solar Cells with Reduced Mobile Ion Concentration and Film Stress. *MRS Commun* **2024**, doi:10.1557/s43579-023-00510-7.
- 30. Guo, Y.; Shoyama, K.; Sato, W.; Nakamura, E. Polymer Stabilization of Lead(II) Perovskite Cubic Nanocrystals for Semitransparent Solar Cells. *Adv Energy Mater* **2016**, *6*, doi:10.1002/aenm.201502317.
- 31. Prochowicz, D.; Tavakoli, M.M.; Solanki, A.; Goh, T.W.; Pandey, K.; Sum, T.C.; Saliba, M.; Yadav, P. 410 Understanding the Effect of Chlorobenzene and Isopropanol Anti-Solvent Treatments on the Recombination 411 and Interfacial Charge Accumulation in Efficient Planar Perovskite Solar Cells. *J Mater Chem A Mater* 2018, 6, 412 14307–14314, doi:10.1039/c8ta03782e.
- 32. An, Y.; Zhang, N.; Zeng, Z.; Cai, Y.; Jiang, W.; Qi, F.; Ke, L.; Lin, F.R.; Tsang, S.W.; Shi, T.; et al. Optimizing Crystallization in Wide-Bandgap Mixed Halide Perovskites for High-Efficiency Solar Cells. *Advanced Materials* **2023**, doi:10.1002/adma.202306568.
- 33. Campanari, V.; Martelli, F.; Agresti, A.; Pescetelli, S.; Nia, N.Y.; Di Giacomo, F.; Catone, D.; O'Keeffe, P.; Turchini, S.; Yang, B.; et al. Reevaluation of Photoluminescence Intensity as an Indicator of Efficiency in Perovskite Solar Cells. *Solar RRL* **2022**, *6*, doi:10.1002/solr.202200049.
- 34. Ye, T.; Zhou, B.; Zhan, F.; Yuan, F.; Ramakrishna, S.; Golberg, D.; Wang, X. Below 200 °C Fabrication Strategy of Black-Phase CsPbI3 Film for Ambient-Air-Stable Solar Cells. *Solar RRL* **2020**, *4*, doi:10.1002/solr.202000014.
- 35. Lou, H.; Lin, C.; Fang, Z.; Jiang, L.; Chen, X.; Ye, Z.; He, H. Coexistence of Light-Induced Photoluminescence Enhancement and Quenching in CH3NH3PbBr3 Perovskite Films. *RSC Adv* **2020**, *10*, 11054–11059, doi:10.1039/d0ra00605j.
- 36. Fiorentino, F.; Albaqami, M.D.; Poli, I.; Petrozza, A. Thermal- and Light-Induced Evolution of the 2D/3D Interface in Lead-Halide Perovskite Films. *ACS Appl Mater Interfaces* 2022, 14, 34180–34188.

37.	Divitini, G.; Cacovich, S.; Matteocci, F.; Cinà, L.; Di Carlo, A.; Ducati, C. In Situ Observation of Heat-Induced
	Degradation of Perovskite Solar Cells. Nat Energy 2016, 1.

ual au- 430 ury to 431

427428429

432

Disclaimer/Publisher's Note: The statements, opinions and data contained in all publications are solely those of the individual author(s) and contributor(s) and not of MDPI and/or the editor(s). MDPI and/or the editor(s) disclaim responsibility for any injury to people or property resulting from any ideas, methods, instructions or products referred to in the content.